Sn_3O_4@TiO_2 CORE-SHELL SURFACES PREPARED BY LIQUID-PHASE DEPOSITION FOR PHOTOELECTROCHEMICAL CELL APPLICATION

by

Margery Elayne Purvis

Submitted in partial fulfillment of the

requirements for Departmental Honors in

the Department of Chemistry and Biochemistry

Texas Christian University

Fort Worth, Texas

May 3, 2021

Sn_3O_4@TiO_2 CORE-SHELL SURFACES PREPARED BY LIQUID-PHASE DEPOSITION FOR PHOTOELECTROCHEMICAL CELL APPLICATION

Project Approved:

Supervising Professor: Benjamin D. Sherman, Ph.D.

Department of Chemistry and Biochemistry

Kayla Green, Ph.D.

Department of Chemistry and Biochemistry

Ashley Wellman, Ph.D.

Department of Criminal Justice

ABSTRACT

Dye-sensitized solar cells represent a promising way to harness solar energy. Core-shell dye-sensitized solar cells are an effective strategy for improving the photoelectrochemical performances of these devices. DSSCs offer lower production cost than the traditional crystalline silicon solar cells and are relatively simple to fabricate. Traditionally, mesoporous titanium(IV) oxide has been used in DSSCs with good results. However, other oxide materials are also of interest and can have more favorable characteristics than their titanium counterparts. In this study, heterovalent tin oxide photoanodes are fabricated and used in dye-sensitized solar cells. Core-shell photoanodes are prepared by adding a shell layer of TiO_2 prepared via liquid-phase deposition on top of a heterovalent tin oxide layer. Liquid-phase deposition of titanium(IV) oxide is a fast and low-cost alternative to atomic layer deposition that still allows for control of layer thickness. The thickness and other surface characteristics of the liquid-phase deposition are optimized prior to their use in dye-sensitized solar cells. The Sn_3O_4@TiO_2 core-shell design is an ideal composition due to the thermodynamically favorable energy gradient from the band gap structure of the species that encourages the flow of electrons from the dye to the shell and the core. The Sn_3O_4@TiO_2 dye-sensitized solar cells demonstrate improved photoelectrochemical performance over Sn_3O_4 DSSCs. However, Sn_3O_4@TiO_2 dye-sensitized solar cells are significantly outperformed by the traditional mesoporous TiO_2 devices.

ACKNOWLEDGMENTS

I would like to express my deepest appreciation to my supervising professor, Dr. Benjamin Sherman. His guidance, mentorship, and support throughout this project and my time in the Sherman Research Group has helped me grow as both a person and a scientist. I would also like to say thank you to the members of the Sherman Research Group, past and present. They have provided much needed support, advice, and comic relief during my most stressful times. I would also like to thank and acknowledge Dr. Bob Neilson. Although he is no longer with us, I owe him my gratitude for being a dedicated and supportive academic advisor and friend. Without him, this project would never have been started. I would like to acknowledge and thank my committee members, Dr. Kayla Green of the Department of Chemistry and Biochemistry and Dr. Ashley Wellman of the Department of Criminal Justice, for taking the time out of their busy schedules to help further my scholarly advancement. In addition, I would like to thank Texas Christian University, the Department of Chemistry and Biochemistry, and the John V. Roach Honors College for allowing me the opportunity to complete this project. Lastly, I would like to thank the Texas Christian University Science and Engineering Research Center for funding this project.

TABLE OF CONTENTS

LIST OF FIGURES

LIST OF TABLES

INTRODUCTION

The sun has been providing energy to the earth's population since they came into existence. Over time, mankind has developed ways to use sources of energy, such as fossil fuels, to satisfy its needs. There are some issues that come from using fossil fuels as the main source of energy for the population. Mainly, the use of fossil fuels has led to issues like global warming, caused by the greenhouse effect from the emission of carbon dioxide during the combustion of the fossil fuels.[1] Proactive research into alternative energy is needed so that a solution can be found before it gets worse. Forms of alternative energy include wind energy, hydroelectric energy, and solar energy. Historically, high costs have hindered the widespread use of solar and wind energy, but the development of new lower-cost technologies have made their use more extensive.[2]

Edmond Becquerel, inspired by Daguerreotype photography, began the field of solar energy research with the discovery of the photovoltaic effect in 1839.[3] In the photovoltaic effect, a photon from light interacts with an electron in a material and can induce photovoltage and photocurrent. This concept is used in solar energy in order to produce an electrical current. Solar energy is a promising form of alternative energy and needs to be investigated further. The earth receives 10,000 times more energy, 3×10^{24} Joules per year, than human civilization uses in that time.[3] Finding a way to harness this energy is the key to using solar energy as a viable alternative for fossil fuels.

Since Becquerel's discovery of the photovoltaic effect, many different types of solar energy devices have been created. Solar energy devices, or solar cells, convert electromagnetic energy from the sun to electrical energy. First-generation solar cells used crystalline silicon and achieved high efficiencies but with relatively high cost. Second-generation solar cells are manufactured from thin films. They require less material but more surface area to produce the substantial

amounts of power when compared to the first-generation. Third-generation solar cells make an effort to improve power conversion efficiency from first-generation while maintaining the thin film architecture and offer lower production cost compared to second-generation cells.[4] They include perovskites, quantum dot-based cells and dye-sensitized solar cells (DSSCs).[4] Fourth-generation solar cells combine low cost surfaces with novel inorganic and organic materials like metal nanoparticles and graphene.[5]

In 1991, Brian O'Regan and Michael Grätzel reported the first DSSCs.[6] They realized that the cost of solar panels was too high for them to become more commonly used and tried to find a new alternative. Using a thin film of mesoporous titanium(IV) oxide (TiO_2) and a ruthenium-based photosensitizer (dye), they made a DSSC. The layer of TiO_2 had a large surface due to its porosity, which allowed for increased dye adsorption when compared to the previous dye-sensitized surfaces which were planar. This resulted in an increased power conversion efficiency and photocurrent.[6] Thus, the DSSCs became a promising direction in solar energy research.

Dye-sensitized solar cells are comprised of numerous components that are built into a small device. The photoanode contains a semiconductor layer and a photosensitized dye on transparent, conductive glass (i.e., fluorine-doped tin oxide glass, FTO). The photoanode is glued to a counter electrode, which is usually platinum on FTO. The space between the sealed electrodes contains an electrolyte solution, usually the iodide/triiodide redox couple.[7]

Dye-sensitized solar cells function using a mechanism based on Becquerel's photovoltaic effect. They operate in a regenerative manner, as seen in the functional diagram in Figure 2. First, photons from light with wavelength and energy related by $E = \frac{hc}{\lambda}$ (E is energy, h is Planck's constant, c is the speed of light in a vacuum, and λ is the wavelength), are absorbed by the dye which promotes an electron from the ground to the excited state. The excited electron is then

injected into the conduction band (CB) of the semiconductor layer, which is lower in energy than the excited state of the dye and leaves the oxidized dye on the surface. Thus, consideration should be taken when choosing the dye. In this study, the **N3** dye is used, and its structure can be seen in Figure 1.[8] The electrons travel through the semiconductor layer, through an external circuit and to the counter electrode. The electron is then used to reduce triiodide from the electrolyte solution to iodide. The iodide is oxidized by the dye cation formed after photoinjection and the process starts over.[9] For the process to work, the ground state of the dye should be lower in energy than the redox couple.[7]

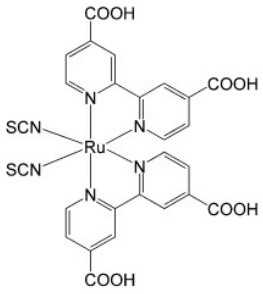

Figure 1. Structure of **N3** dye.

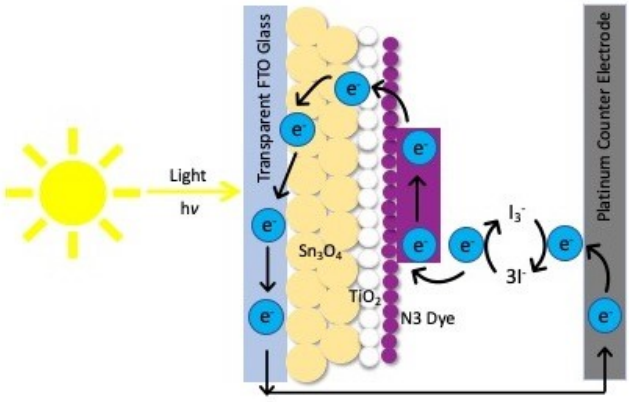

Figure 2. Functional diagram of a dye-sensitized solar cell.

The dye-sensitized solar cell seen in Figure 2 is an example of a core-shell dye-sensitized solar cell. In DSSCs, one factor that leads to low performance is charge recombination.

Recombination occurs when an injected electron goes back to the hole in the dye and does not travel through the device. Thus, the power conversion efficiency and photocurrent of the device is decreased. The strategic addition of a semiconductor shell layer provides an energy barrier between the core and the dye and prevents recombination.[10]

In dye-sensitized solar cells, the dye is the chromophore, or light absorber, and provides the excited electrons that are involved in photocurrent flow. This leaves flexibility when choosing the semiconductor layer. The highest performing dye-sensitized solar cells utilize mesoporous titanium(IV) oxide, the material O'Regan and Grätzel used in their first device.[6] It is low cost, non-toxic, and is widely used in a variety of applications.[11] Mesoporous surfaces have numerous benefits for use in dye-sensitized solar cells. They have a low distance for electron diffusion, are crystalline enabling rapid charge transport, and have high surface area to allow for increased adsorption of the photosensitized dye.[12] Numerous mesoporous materials have been used for semiconductors in dye-sensitized solar cells, including TiO_2, zinc oxide (ZnO), and tin(IV) oxide (SnO_2).[13]

When choosing a semiconductor to use in a dye-sensitized solar cell, it should have key properties that will result in a functioning device. Low cost, high electron mobility, high electron injection rate, and facile synthesis are a few of the desirable characteristics.[14] Recently, the use of tin oxide materials has been investigated because they have desirable band gaps and electron transport properties.[15] Furthermore, nonstoichiometric tin oxides like Sn_3O_4 have gained recent interest.[16] SnO_2 has a wider band gap than both Sn_3O_4 and TiO_2.[17]

Heterovalent tin oxide, or Sn_3O_4, was first characterized in 1967.[18] The material is a combination of tin in different oxidation states: Sn_3O_4 contains two atoms of tin(II) for each atom of tin(IV).[17] Current research involving this material has focused on its use as a photocatalyst for

hydrogen gas evolution.[19] This material has not been widely used for dye-sensitized solar cells and its performance needs to be further investigated. It has a lower energy band gap, which enables it to absorb light in the visible region and have favorable band gap properties.[15] The material can be synthesized relatively easily and then prepared into a paste that is applied to the transparent electrode.

Including a shell coating that is deposited on top of a core oxide furthers the available options for photoanode composition. A shell coating serves to prevent electron recombination and direct the flow of electrons away from the dye towards the back contact and onto the counter electrode, thus increasing the photocurrent flow and overall performance of the device. The electrons flow from the excited state of the dye to the conduction band of the shell and then to the conduction band of the core. Conduction band energies of the semiconductors should thermodynamically favor the flow of charge. Therefore, the conduction band of the shell should be lower in energy than the excited state of the dye but higher in energy than the conduction band of the core. Thus, the flow of electrons is directed from the dye to the core. TiO_2 shell-based dye-sensitized solar cells have been investigated previously with good results.[20, 21] This study will focus on the development and optimization of Sn_3O_4@TiO_2 core-shell dye-sensitized solar cells. This is an optimal combination because the potential of the TiO_2 conduction band (-0.5 V vs. NHE)[22] is higher (more negative) than the Sn_3O_4 conduction band (-0.25 V vs. NHE).[23]

A shell layer of TiO_2 can be prepared in different ways, including via atomic layer deposition (ALD) and liquid-phase deposition (LPD).[21] ALD is an expensive process which disagrees with the effort to develop low-cost devices. A reasonable alternative to atomic layer deposition is LPD. The liquid-phase deposition of TiO_2 process used here occurs during a ligand exchange equilibrium reaction of ammonium hexafluorotitanate as seen in Equations 1-4.[24] Boric

acid acts as a fluoride scavenger and drives the equilibrium reaction forward (Equation 4). The TiO_2 crashes out of a supersaturated solution and adheres directly onto the substrate.[24] The liquid-phase deposition procedure needs to be optimized to provide the best opportunity for performance enhancement of the dye-sensitized solar cell.

(1) $[TiF_6]^{2-} + nH_2O \rightleftharpoons [TiF_{6-n}(OH)_n]^{2-} + nHF$

(2) $[TiF_{6-n}(OH)_n]^{2-} + (6-n)H_2O \rightarrow [Ti(OH)_6]^{2-} + (6-n)F^- + (6-n)H^+$

(3) $[Ti(OH)_6]^{2-} + 2H^+ \rightarrow TiO_2 + 4H_2O$

(4) $H_3BO_3 + 4HF \rightleftharpoons HBF_4 + 3H_2O$

The surfaces that make up dye-sensitized solar cells and the devices themselves can be characterized in many ways. The materials can be analyzed using UV-vis spectroscopy, profilometry, scanning electron microscopy (SEM), transmission electron microscopy (TEM), and energy dispersive X-ray spectroscopy (EDX). UV-vis spectroscopy investigates the absorption of ultraviolet and visible light by the material, profilometry investigates the thickness of the surface, scanning electron microscopy investigates the surface morphology and topology of the surface, and transmission electron microscopy investigates the crystallinity of the material. The devices can be characterized and analyzed for their photoelectrochemical performance using chronoamperometry and linear sweep voltammetry. Chronoamperometry (CA) investigates the photocurrent generation of the device when it is illuminated with light; linear sweep voltammetry (LSV) investigates the open circuit potential (V_{OC}), short circuit current density (J_{SC}), fill factor (FF), maximum power (P_{MAX}), and power conversion efficiency (η) of the device when it is illuminated with light.

There are many factors that can be investigated to gauge the performance of a dye-sensitized solar cell. From chronoamperometry, the photocurrent that is generated under

illumination is measured and should be maximized. From linear sweep voltammetry, parameters such as short circuit current, open circuit potential, fill factor, maximum power, and power conversion efficiency can be determined. The fill factor is a ratio of the maximum power output of the device and the theoretical maximum power output of the cell based on the open circuit potential and the short circuit current. The power conversion efficiency is a ratio of the maximum power of the cell and the input power from the light source. Formulas for these parameters can be found in Equations 5 and 6.[25] All of these parameters should be maximized.

(5) $$\eta = \frac{P_{MAX}}{P} = \frac{J_{MP} \times V_{MP}}{P}$$

(6) $$FF = \frac{P_{MAX}}{J_{SC} \times V_{OC}} = \frac{J_{MP} \times V_{MP}}{J_{SC} \times V_{OC}}$$

In this study, Sn_3O_4@TiO_2 core-shell DSSCs are prepared and their photoelectrochemical performance is evaluated. Various analytical and qualitative techniques are used to characterize the Sn_3O_4@TiO_2 photoanodes and TiO_2 shell layers prepared via the liquid-phase deposition method. The presence of TiO_2 on a Sn_3O_4 surface after TiO_2 LPD treatment is confirmed and the liquid-phase deposition procedure is optimized to produce a uniform film. A reliable procedure to control the properties of the shell coating is developed by generating a growth curve of TiO_2 thickness as a function of reaction temperature and time. Addition of an optimized TiO_2 shell layer improves the photoelectrochemical performance of Sn_3O_4-based DSSCs by reducing recombination due to the thermodynamically favorable energy gradient of the core-shell design.

EXPERIMENTAL

General Information

The protocol for the synthesis of heterovalent tin oxide, Sn_3O_4, was adapted from Tanabe et al.[17] The protocol for the titanium(IV) oxide layer, TiO_2, was adapted from Yu et al.[24] In this

project the following chemical reagents were used: tin(II) chloride dihydrate ($SnCl_2•2H_2O$), sodium citrate dihydrate ($Na_3C_6H_5O_7•2H_2O$), sodium hydroxide (NaOH), hydrochloric acid (HCl), glacial acetic acid (CH_3COOH), 100,000 molecular weight poly(ethylene oxide) (PEO), 12,000 molecular weight poly(ethylene glycol) (PEG), boric acid (H_3BO_3), ammonium hexafluorotitanate ($(NH_4)_2TiF_6$), iodine (I_2), lithium iodide (LiI), 1,3-dimethylimidazolium iodide ($C_5H_9IN_2$), guanidine thiocyanate (CH_6N_3SCN), 4-*tert*-butylpyridine ($C_9H_{13}N$), chloroplatinic acid (H_2PtCl_6), and **N3** ruthenium dye (*cis*-bis(isothiocyanato)bis(2,2'-bipyridyl-4,4'dicarboxylato) ruthenium(II)), whose chemical structure can be found in Figure 1. Solvents used in this project include millipure water, ethanol, valeronitrile, and acetonitrile. Nitrogen gas (N_2) was used as a drying agent. Fluorine-doped tin oxide glass (FTO) was used as the substrate and Meltonix 1170-25 thermoplastic sealing film (Solaronix) was used to construct the solar cell.

UV-vis spectra were acquired with an Agilent Technologies Cary 60 spectrophotometer. Measurements to gauge photovoltaic performance were acquired using a Sciencetech SLB300B collimated solar simulator and a Keithley 2450 SourceMeter. Scanning electron microscopy images were obtained with JEOL JSM-7100 F. Surface thickness measurements were obtained with a Bruker Dektak XT. Transmission electron microscopy images and EDX spectra were obtained with a JEOL JEM-2100 with an accelerating voltage of 200 kV. Instruments used during the project also include a Branson M3800H ultrasonication bath, Hettich Zentrifugen Universal 320 centrifuge, Heidolph rotary evaporator, Parr Instruments model 4744 45 mL reaction vessel, and Thermo Scientific Lindberg Blue M model BF51894C-1 box furnace. Components of this project were obtained from Alfa Aesar, Beantown Chemical, Praxair, Sigma-Aldrich, Hartford Glass Company, and Solaronix.

Synthesis of Heterovalent Tin Oxide – Sn_3O_4

Millipure water (17 mL) and 9 mL of 0.420 M sodium citrate dihydrate (3.78 mmol) were combined and then sonicated for 5 minutes. Tin(II) chloride dihydrate (0.338 g, 1.50 mmol) was added to the same beaker and sonicated until dissolved, giving a 2.5:1 mole ratio of citrate to tin. The pH of the solution was adjusted between 8.05 and 8.20 with dilute sodium hydroxide or hydrochloric acid solution as needed. The beaker was sonicated again to ensure the solution was thoroughly mixed giving an opaque, white solution. Exactly 30 mL of the solution was transferred to the Parr reactor. After assembling the reactor, it was placed in the box furnace. The furnace was set to ramp up from room temperature (25 ℃) to 180 ℃ in one hour (about 2.6 ℃/min) then hold at 180 ℃ for 6 hours before returning to room temperature.

After the reactor had cooled to room temperature, the Teflon liner of the reactor was sonicated to dislodge any particles from the liner wall and thoroughly mix the contents. After the hydrothermal reaction is complete, the reactor should contain pale yellow particles (Sn_3O_4) in a liquid that has a pearly sheen. The contents were transferred to a centrifuge tube and the liner was rinsed to transfer all particles. After balancing the centrifuge, the tube was centrifuged for 10 minutes at 8000 RPM. The supernatant was removed and millipure water was added until the particles were covered by about an inch, and then were centrifuged again for 10 minutes at 8000 RPM to wash the particles. This process was repeated once with ethanol and once with a 50/50 mixture of millipure water and glacial acetic acid.

The particles were then resuspended in 5 mL of glacial acetic acid and transferred to a scintillation vial. The vial was attached to the rotary evaporator and the volume of liquid was reduced almost completely. The scintillation vial with the Sn_3O_4 particles was placed in a

desiccator that was attached to a vacuum pump and were dried for about 4 hours to obtain the clean, dry, yellow final product.

Preparation of Sn_3O_4 Paste

Paste used to fabricate high surface area electrodes was prepared by combining 100 mg each of PEG and PEO with 84.0 mg Sn_3O_4 (0.200 mmol) in a small vial to give 9 wt% of both polymer (100 mg/mL) and 8 wt% (84 mg/mL) of Sn_3O_4. The dry materials were added to 0.900 mL ethanol and 0.100 mL glacial acetic acid. A small stir bar was placed in the vial and the paste was stirred for at least 48 hours prior to the fabrication of electrodes.

Photoanode Fabrication with Sn_3O_4 Paste

FTO glass was cut into 1 × 4 cm rectangles and then washed with ethanol in a sonication bath. The Sn_3O_4 paste was applied to the conductive side of the FTO using the 'doctor blading' method.[26] After the film air dried, the electrodes were sintered in the box furnace at 450 ℃ for 45 minutes (10 ℃/min ramp rate used to reach temperature).

Addition of Titanium(IV) Oxide Layer

Ammonium hexafluorotitanate (100 mg, 0.505 mmol) was dissolved in 10 mL of 0.3 M boric acid (3 mmol) in a scintillation vial, giving a 1:6 molar ratio of titanium to boric acid. The previously fabricated Sn_3O_4 electrodes or bare FTO were placed in small vials, and then 2 mL of the $H_3BO_3/(NH_4)_2TiF_6$ solution was added to each vial. The electrodes were left in the solution for varying amounts of time which depended on the desired thickness of the layer. This experiment was carried at 25 °C, 35 °C, and 45 °C. The resultant electrodes were characterized using surface profilometry, SEM imaging, EDX analysis, and UV-Vis spectroscopy.

*Sensitization of the Photoanode with **N3** Dye*

A 300 μM solution of **N3** dye was prepared by dissolving 2.67 mg of **N3** powder (3.60 nmol) in 12 mL of ethanol. The fabricated electrodes were immersed in the solution for 24 hours, then removed and allowed to dry. The dye adsorbed to the surface and changed the color of the electrodes to a salmon color.

Platinum Counter Electrode Fabrication

A 0.01 M chloroplatinic acid solution was prepared in ethanol. After the solution was prepared, 20 μL of solution was pipetted onto the conductive side of a clean piece of FTO glass. The FTO was dried and then another layer of chloroplatinic acid was deposited in the same way. After completely dry, the FTO was placed into a box furnace. The furnace was set to ramp up to 450 ℃ in 45 minutes and then hold at 450 ℃ for 45 minutes before returning to room temperature. The end product is the FTO with a platinum surface layer. Two holes were drilled into the electrode to allow introduction of an electrolyte solution at a later point.

Dye Sensitized Solar Cell Construction

The photoanode and platinum counter electrode were sealed together using thin strips of the Meltonix film. An electrolyte comprised of 0.03 M I_2, 0.05 M LiI, 1.0 M 1,3-dimethylimidazolium iodide, 0.1 M guanidine thiocyanate, and 0.5 M 4-*tert*-butylpyridine dissolved in a 50/50 mixture of acetonitrile and valeronitrile was added to the cell through the holes drilled in the platinum electrode. A 1 × 2 cm microscope slide was placed over the drilled holes and secured using small pieces of Parafilm.

Dye Sensitized Solar Cell Evaluation

Each device was constructed following the procedure outlined above and was secured in front of the light source for solar simulations. The device was placed to receive an illumination

intensity of 1 sun (100 mW/cm^2), which was about 9 inches from the light source. The DSSC was irradiated with the artificial sun and the resultant current and potential were measured with the multimeter. Various experiments were run on the devices. Linear voltage sweep experiments (LSV) were conducted under the artificial sunlight to determine the resultant current under a specific potential. Chronoamperometry (CA) experiments were conducted by turning the artificial sunlight on and off and measuring the resultant current at constant 0 V applied bias. The short circuit current, open circuit potential, fill factor, maximum power, and power conversion efficiency of each cell were determined.

RESULTS

Titanium(IV) Oxide Layer Characterization

Photographs of the thickest layers of TiO_2 films on microscope slides can be found in Figure 3. The images show that more transparent films result from the reaction run at a lower temperature. The films produced at higher temperature are more opaque than the films produced at lower temperature.

A plot of the thickness of the TiO_2 layer versus time for the different reaction temperatures can be found in Figure 4. The plot shows that when the reaction is carried out at high temperatures, there is faster increase in thickness of the TiO_2 layer. When the temperature of the reaction increases by ten degrees, the TiO_2 layer growth rate roughly doubles.

Figure 5 shows SEM images of the layers. These images were taken of the ~ 100 nm samples at different magnifications. The images show that as the temperature of the reaction increases, the layers are less uniform and there are larger aggregates of particles on the surface. Cracking of the samples occurred at temperatures of 35 °C and 45 °C. Figure 6 shows the UV-vis spectra of the ~ 100 nm films. The absorbance increases slightly with an increase in temperature.

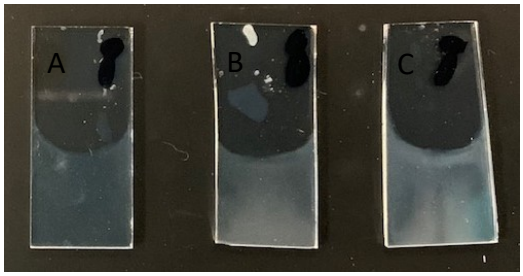

Figure 3. Photographs of the 100 nm TiO_2 films prepared at (A) 25 °C, (B) 35 °C, and (C) 45 °C.

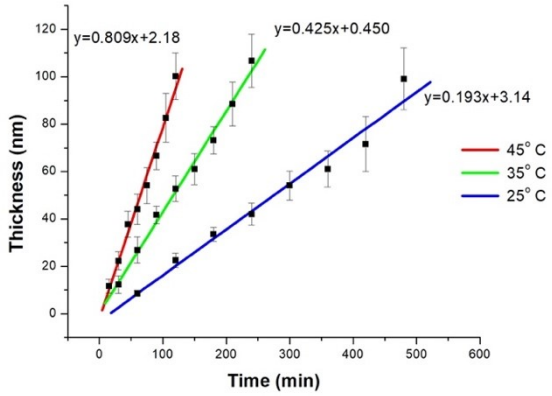

Figure 4. Growth of TiO_2 films on FTO using a 0.05 M solution of TiF_6^{2-}. The films were prepared under different reaction temperatures of 45 °C (red), 35 °C (green), and 25 °C (blue). Surface thicknesses were determined using profilometry measurements and each point is the average of five independent sample measurements.

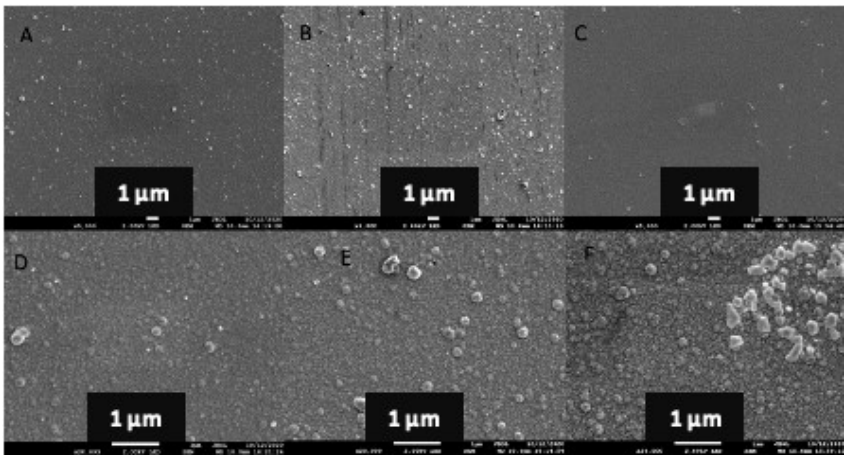

Figure 5. SEM images of TiO_2 films prepared from 0.05 M TiF_6^{2-} at 25 °C (A and D), 35 °C (B and E), and 45 °C (C and F). The scale bars are 1 µm.

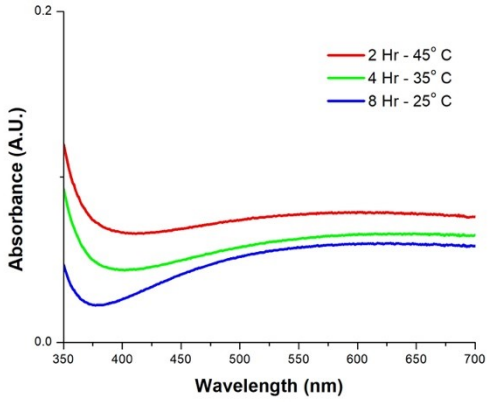

Figure 6. UV-vis spectra of the TiO_2 films prepared from 0.05 M TiF_6^{2-} with reaction times of 2 hours at 45 °C (red), 4 hours at 35 °C (green), and 8 hours at 25 °C (red).

Photoanode Fabrication and Characterization

Figures 7 and 8 show images of the Sn_3O_4 powder and paste used in the electrode fabrication. Figures 9-11 show images of the different iterations of photoanodes used in this study. The dyed electrode has a noticeably different color than the undyed electrode. The dyed electrode turned a pink-salmon color (right-most image in Figure 9). Figure 10 shows the Sn_3O_4 electrode with 5 nm of TiO_2 at different stages of fabrication up to the final dyed surface. Again, the dyed

electrode is a noticeably different color than the undyed electrode. The electrode turned a darker pink than the electrode without any TiO_2. In Figure 11, the Sn_3O_4 electrode with 10 nm of TiO_2 is fabricated and then dyed. The electrode turned a darker pink than both the electrode with 5 nm TiO_2 and the electrode without any TiO_2. UV-vis spectra of the film progression can be found in Figure 12.

Figure 13 shows TEM images of the Sn_3O_4@TiO_2 electrodes with 5 nm of TiO_2 taken at different magnifications. The images show the darker sheet-like Sn_3O_4 with a lighter layer of TiO_2 around it. The EDX spectrum of the Sn_3O_4@TiO_2 electrode with 5 nm of TiO_2 can be found in Figure 14. The plot indicates the presence of tin and titanium.

Figure 7. The synthesized Sn_3O_4 powder.

Figure 8. The Sn_3O_4 paste prepared with the powder from Figure 7.

Figure 9. Photographs of the progression of a Sn_3O_4 photoanode from (A) the undyed surface to (B) the dyed sample.

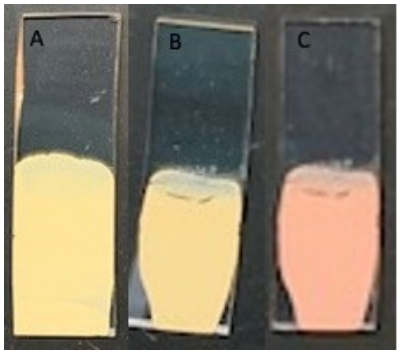

Figure 10. Photographs of the progression of a 5 nm TiO_2 coated Sn_3O_4 photoanode: (A) after Sn_3O_4 film deposition, (B) after addition of a 5 nm TiO_2 coating, and (C) after soaking in a solution of **N3**.

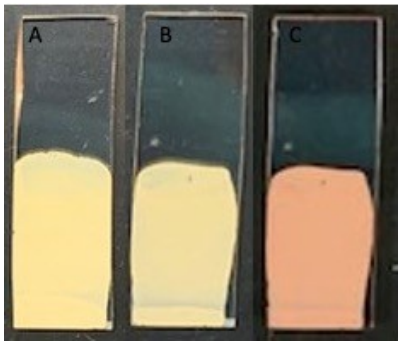

Figure 11. Photographs of the progression of a 10 nm TiO_2 coated Sn_3O_4 photoanode: (A) after Sn_3O_4 film deposition, (B) after addition of a 10 nm TiO_2 coating, and (C) after soaking in a solution of **N3**.

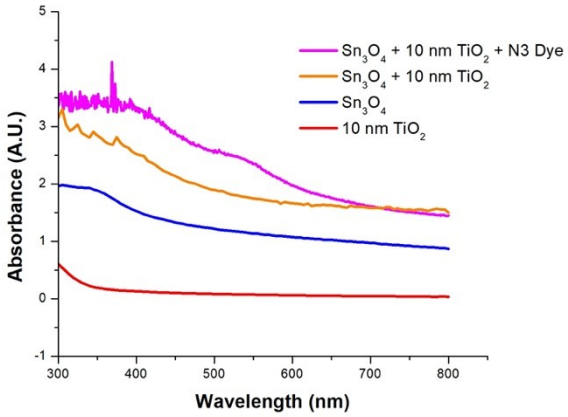

Figure 12. UV-vis spectra of the photoanode films.

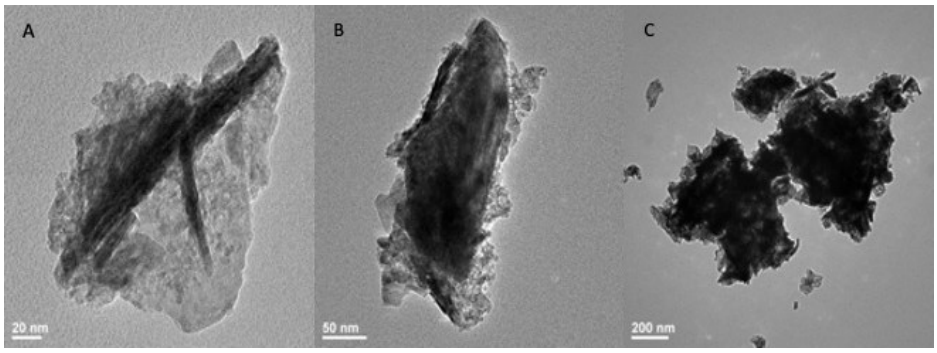

Figure 13. TEM images of the Sn_3O_4@TiO_2 films with estimated TiO_2 thickness of 5 nm at different magnifications: (A) has scale bar of 20 nm, (B) has a scale bar of 50 nm, and (C) has scale bar of 200 nm.

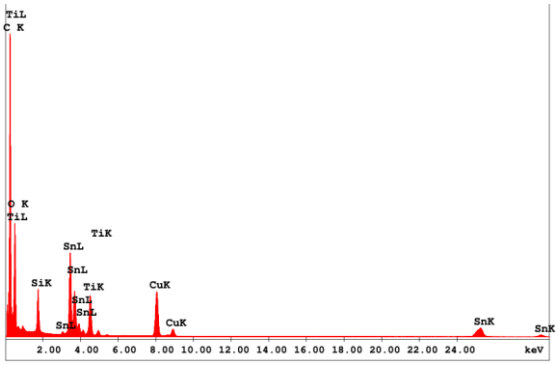

Figure 14. EDX spectrum of the Sn_3O_4@TiO_2 film with estimated TiO_2 thickness of 5 nm.

Photoelectrochemical Studies

A photo of an example dye sensitized solar cell can be found in Figure 15. Linear sweep voltammograms of each type of DSSC can be found in Figure 16. Chronoamperograms of each type of DSSC can be found in Figure 17. Light on and off cycles lasted 30 seconds each and the experiment was conducted for 210 seconds under 0 V applied bias. All DSSCs were evaluated under an intensity of 1 sun. The average results from these experiments are found in Table 1, including the open circuit potential, short circuit current, maximum power, fill factor, and power conversion efficiency for each cell type.

Figure 15. Photograph of example DSSCs.

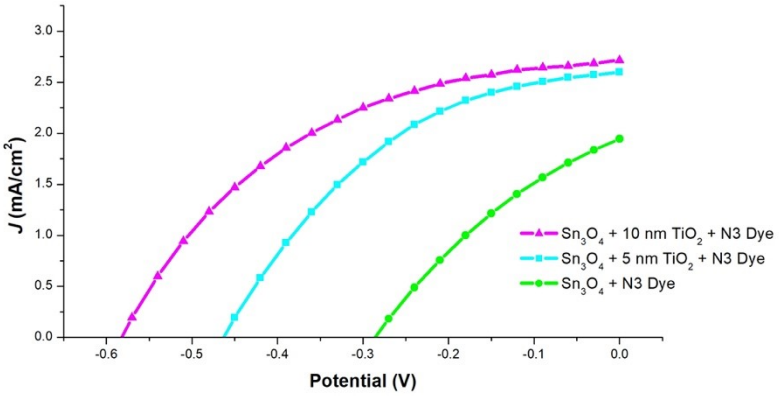

Figure 16. Linear sweep voltammograms for the different types of DSSCs when evaluated under an intensity of 1 sun.

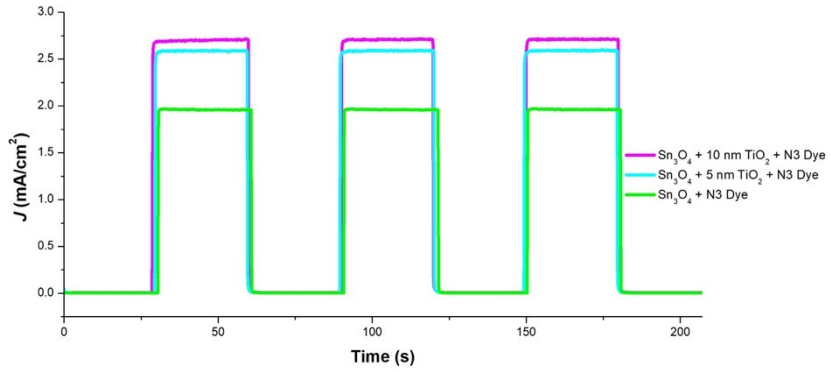

Figure 17. Chronoamperograms for the different types of DSSCs when evaluated under an intensity of 1 sun and 0 V applied bias. Each light on and light off period lasted 30 seconds for a total time of 210 seconds.

Table 1. Photoelectrochemical Performance of the Different Types of DSSCs Studied.

DSSC Type	V_{OC} (V)	J_{SC} (mA/cm^2)	P_{MAX} (mW/cm^2)	FF (%)	η (%)
Sn_3O_4 + 10 nm TiO_2	-0.58 ± 0.04	2.7 ± 0.3	0.68 ± 0.02	44 ± 4	0.68 ± 0.02
Sn_3O_4 + 5 nm TiO_2	-0.45 ± 0.06	2.6 ± 0.02	0.4 ± 0.1	37 ± 4	0.4 ± 0.1
Sn_3O_4	-0.27 ± 0.01	2.0 ± 0.4	0.19 ± 0.02	34 ± 2	0.19 ± 0.02

DISCUSSION

Titanium(IV) Oxide Layer Characterization

The titanium(IV) oxide surfaces prepared with liquid-phase deposition were analyzed using profilometry, SEM, and UV-vis spectroscopy. Profilometry provides an estimation of the thickness of the surface. The thickness can be used to generate growth curves as a reliable method to control the thickness of a film. SEM imaging provides a close look into the morphology and characteristics of the surface of the film. This can provide key information about the surface and can explain some of the behavior of the film. UV-vis spectroscopy can provide insight into the interaction of light with the surface. The films prepared at various temperatures were characterized

in order to determine the optimal conditions for preparation of films for use in the dye-sensitized solar cells in this project.

Figure 3 is an image of the films after the longest time point at each temperature. Apparent by eye, the films grow more opaque as the reaction temperature is increased. A change in temperature has effects on the kinetics of a reaction which should cause morphology changes on the surface of the films. The growth curve of the TiO_2 films in Figure 4 show a linear increase in thickness with time. At higher reaction temperatures, there is a faster deposition rate of TiO_2 on the film as evidenced by the increasing slopes. A slower deposition rate should result in more desirable characteristics, such as fewer structural defects and particle aggregates. The films shown in Figure 3 are 100 nm based on this growth curve.

To investigate the surface morphology of the TiO_2 film, SEM imaging was used. Figure 5 depicts the SEM image of the 100 nm films at the longest point for each reaction temperature. Consistent with the observations from the color of films, the SEM images show differences in surface morphology for the films grown at different temperatures. At 25 °C, the films have a more uniform surface area than the ones grown at the higher temperatures. While some particle aggregates are present, these appear smaller and more evenly dispersed than the films formed at higher temperatures. At 35 °C, the films begin to grow larger aggregates and there is evidence of cracking on the surface. At 45 °C, the films have more and larger particle aggregates. The morphology and aggregation of particles on the films is consistent with literature.[27]

The aggregation of particles observed in the SEM images (Figure 5) can cause scattering of incident light and cause the opaque color of the films. UV-vis spectra from Figure 6 show that the absorbance of the films slightly increases despite their similar thicknesses. This could be due

to the incident light being scattered and not reaching the detector, thus leading to a high apparent absorbance.

Scattering of light is not favorable in a dye-sensitized solar cell and should be considered when choosing the photoanode surface material. Incident light should reach the photoanode and scattering would result in a lower power conversion efficiency. A lower reaction temperature leads to more uniform surfaces with crystals that have less impurities and defects. Electrons from the photocurrent generation can get trapped in the defect sites and lead to a lower photocurrent. Based on these factors, the ideal reaction temperature was determined to be 25 °C, and this temperature was used for the liquid-phase deposition reaction for the photoanode shell material in this project.

Photoanode Fabrication and Characterization

The Sn_3O_4 particles and paste from Figures 7 and 8 were used to prepare the photoanodes in Figures 9, 10, and 11. There is no visible difference between a bare Sn_3O_4 surface and a Sn_3O_4 surface that was coated with TiO_2. Figure 9 depicts the progression of the preparation of a dye-sensitized Sn_3O_4 photoanode. The dyed surface is a light salmon color. With the addition of the TiO_2 layer in Figures 10 and 11, the color of the dyed surface darkens which implies that there an increase in dye adsorption to the TiO_2-covered surface. This is favorable because there should be an increased probability of electron excitation and injection from the dye, thus an increase in photocurrent. The surface darkens further with the thicker shell coating of TiO_2. The anchoring groups of the **N3** dye have a thicker layer of TiO_2 to adsorb onto and are more likely to stay attached to the surface when the electrode is immersed into the dye solution.

The UV-vis spectra of the film progression can be found in Figure 12. The spectrum of the TiO_2 layer is mostly flat in the visible region of light and begins absorbing in the ultraviolet region. TiO_2 has a bandgap of 3.2 eV.[28] The energy of the photon that is absorbed by a material

corresponds to the difference between the valence and conduction bands, thus the TiO_2 absorbs in the ultraviolet region. The Sn_3O_4 layer absorbs in the visible region due to its lower energy bandgap of 2.8 eV. This is consistent with its yellow color, which indicates absorption in the blue/purple range of the visible spectrum of light. The Sn_3O_4 films show increased absorbance near 400 nm compared with TiO_2, which agrees with the literature values.[17]

The combination of materials results in an additive effect on the absorbance measurements in the UV-vis spectrum. In the undyed spectrum, there is an increase in absorbance in both the visible and ultraviolet range when compared to either the bare Sn_3O_4 or TiO_2 spectra. The TiO_2 layer absorbs the UV photons while the Sn_3O_4 absorbs photons in the high energy range of the visible region. Combining these two layers causes an addition in absorbance resulting in an increased absorbance across the spectrum. The absorbance in both the ultraviolet and visible region helps to confirm that the TiO_2 layer was deposited on top of the Sn_3O_4 layer.

The majority of light that hits the Earth is in the visible region, so absorbance in the visible region would be optimal for the DSSC. This would result in increased power conversion efficiency and be more practical for real life applications. Addition of the **N3** dye layer shifts the absorbance even further into the visible range. The dye is a dark pink or maroon color, indicating that it absorbs light in the green region. This is consistent with the peak from the dye that is present around 550 nm.

Figure 13 shows the TEM images taken of the Sn_3O_4@TiO_2 coatings with an estimated thickness of 5 nm. Part (A) shows a darker sheet-like species that is consistent with the morphology of the Sn_3O_4 that is presented in literature.[17] The darker sheet-like moiety is coated with a lighter, spherical species that is consistent with the morphology of the TiO_2 synthesized through the liquid-phase deposition process.[24] The thickness of the film is larger than the estimated 5 nm in some

regions, which is expected in some areas due to aggregate formation. Figure 14 shows the EDX spectrum of the Sn_3O_4@TiO_2 films with an estimated 5 nm thickness of TiO_2. The spectrum helps confirm the presence of both titanium and tin in the completed film.

Photoelectrochemical Studies

The photoelectrochemical performance of the DSSCs was evaluated using linear sweep voltammetry and chronoamperometry. The linear sweep voltammograms provide key information used to evaluate the dye-sensitized solar cells. The LSV experiments give the open circuit potential (V_{OC}), short circuit current density (J_{SC}), fill factor (FF), maximum power (P_{MAX}), and power conversion efficiency (η). The chronoamperometry experiments provide the photocurrent density values when the device is under periodic illumination. Comparing the LSV and CA results from the different types of DSSCs can help determine if the photoelectrochemical performance of the DSSCs has improved upon addition of the shell coating of TiO_2.

The linear sweep voltammetry experiments from Figure 15 show an increase in the open circuit potential as the thickness of the TiO_2 shell layer increases. The open circuit potential of the dyed Sn_3O_4 DSSC is -0.27 V. The dyed 5 nm and 10 nm Sn_3O_4@TiO_2 DSSCs have open circuit potentials of -0.45 V and -0.58 V, respectively. A higher magnitude of open circuit potential indicates that the device is more capable of converting solar energy to electrochemical potential energy. Thus, the device can sustain a higher photocurrent. SnO_2 and TiO_2 DSSCs from previous studies have generated open circuit potentials of about -0.34 V and -0.69 V, respectively.[29] SnO_2@TiO_2 core-shell devices have been prepared using different precursors than the procedure explored in this study; $TiCl_4$ as the titanium precursor improved the V_{OC} to 0.40 V.[29] The V_{OC} of the Sn_3O_4@TiO_2 DSSCs are a clear improvement upon SnO_2-based devices but not for TiO_2-based devices.

The LSV experiments in Figure 15 show an increase in the short circuit current of the DSSCs with increasing thickness of the shell layer. The Sn_3O_4 devices have a short circuit current of 2.0 mA/cm^2 while the 5 nm and 10 nm Sn_3O_4 devices have short circuit currents of 2.6 mA/cm^2 and 2.7 mA/cm^2, respectively. The short circuit current of the SnO_2 devices is 2.5 mA/cm^2.[29] Using the $TiCl_4$ precursor for the TiO_2 reduced the short circuit to 1.3 mA/cm^2. The photocurrent density of the Sn_3O_4 DSSCs developed in this study show slightly improved the performance when compared to SnO_2, but not when compared to TiO_2. The J_{SC} of TiO_2-based DSSCs is 6.7 mA/cm^2.[29] However, the short circuit current of the Sn_3O_4@TiO_2 DSSCs is significantly improved when compared to Sn_3O_4 DSSCs.

The maximum power, fill factor, and power conversion efficiency of the DSSCs from this project were calculated using Equations 4 and 5. The P_{MAX}, FF, and η of the DSSCs improved with increased thickness of the TiO_2 shell layer. The max power and power conversion efficiency were about doubled with introduction of a 5 nm shell coating and more than tripled with a 10 nm shell coating. This is a clear advantage of using a shell coating of TiO_2. The fill factor of the Sn_3O_4@TiO_2 DSSCs are also an improvement: 34% for Sn_3O_4, 37% for a 5 nm shell coating, and 44% for a 10 nm shell coating. The use of a Sn_3O_4@TiO_2 interface is clearly advantageous over Sn_3O_4 for maximum power, power conversion efficiency, and fill factor. However, the mesoporous TiO_2-based devices are superior for every parameter.[29] The Sn_3O_4@TiO_2 DSSCs outperform SnO_2, but the SnO_2 DSSC outperforms the Sn_3O_4. Combining a TiO_2 layer with SnO_2 led to a reduced fill factor (45% vs. 39%).[29]

Overall, there is an improvement in performance of the Sn_3O_4 DSSCs when a shell layer of TiO_2 is added. This is a promising trend. This improved performance is consistent with the thermodynamically favorable conduction band gradient established at the photoanode interface.

The addition of the shell coating decreases recombination and drives current down the energy gradient. Thus, the photocurrent and other DSSC parameters are maximized. Additionally, there is an increase in adsorption of the **N3** dye when the TiO_2 shell coating is present. Consequently, an improvement is expected due to a higher surface coverage of the chromophore.

On the contrary, combining a TiO_2 shell layer using $TiCl_4$ precursors limits the fill factor of the SnO_2@TiO_2 devices. However, there is still an improvement in the V_{OC}, J_{SC}, and η. Additionally, SnO_2@TiO_2 devices using TiF_6^{2-} precursors with a thin blocking layer of denser SnO_2 between mesoporous paste layer and the FTO have been examined in other studies.[29] There is a consistent increase in performance for V_{OC}, J_{SC}, and η in these devices. Using this third layer in the Sn_3O_4@TiO_2 devices may enhance the photoelectrochemical performance even more provided the thermodynamically favorable design is maintained.

CONCLUSION

In this study, heterovalent tin oxide is synthesized and used as the oxide layer in dye-sensitized solar cells. Sn_3O_4@TiO_2 core-shell dye-sensitized solar cells were fabricated using the liquid-phase deposition procedure of TiO_2. The thickness of the shell layer was investigated, and the reaction temperature was optimized to fabricate a smooth, uniform surface morphology for the DSSC surface. The optimal reaction temperature was determined to be 25 °C, likely due to the slower growth rate causing slower crystal growth and aggregate formation. The Sn_3O_4@TiO_2 core-shell design was chosen to generate a thermodynamically favorable energy gradient to encourage the flow of electrons from the dye to the back contact and the counter electrode.

Overall in this study, the Sn_3O_4@TiO_2 dye-sensitized solar cells demonstrate improved photoelectrochemical performance over Sn_3O_4 DSSCs. This is consistent with the thermodynamically favorable gradient; the conduction bands of Sn_3O_4 and TiO_2 are -0.25 V versus

NHE[23] and -0.5 V versus NHE[22], respectively. The conduction band of the TiO_2 is higher (more negative) than the conduction band of Sn_3O_4, thus the electrons travel down the gradient before returning to the dye. However, Sn_3O_4@TiO_2 dye-sensitized solar cells are significantly outperformed by mesoporous TiO_2 devices, thus additional modifications need to be applied to the Sn_3O_4@TiO_2 devices.

REFERENCES

1. Solomon, S., Plattner, G. K., Knutti, R., Friedlingstein, P., Irreversible climate change due to carbon dioxide emission. *Proc. Natl. Acad. Sci.* **2009,** *106* (6), 1704-1709.
2. Gielen, D., Boshell, F., Saygin, D., Bazilian, M. D., Wagner, N., Gorini, R., The role of renewable energy in the global energy transformation. *Energy Strategy Rev.* **2019,** *24*, 38-50.
3. Grätzel, M., Photoelectrochemical cells. *Nature* **2001,** *414*, 338-345.
4. Bagher, A. M., Abadi Vahid, M. M., Mohsen, M., Types of Solar Cells and Application. *Amer. J. Opt. Photonics* **2015,** *3*, 94-113.
5. Ikpesu, J. E.; Iyuke, S. E.; Daramola, M.; Oyetunde, O. A., Synthesis of improved dye-sensitized solar cell for renewable energy power generation. *J. Sol. Energy* **2020,** *206*, 918-934.
6. O'Regan, B.; Gratzel, M., A low-cost, high-efficiency solar cell based on dye-sensitized colloidal TiO_2 films. *Nature* **1991,** *353*, 737-740.
7. Sharma, K.; Sharma, V.; Sharma, S. S., Dye-Sensitized Solar Cells: Fundamentals and Current Status. *Nanoscale Res. Lett.* **2018,** *13* (1), 381.
8. Ito, S., Investigation of Dyes for Dye-Sensitized Solar Cells: Ruthenium-Complex Dyes, Metal-Free Dyes, Metal-Complex Porphyrin Dyes and Natural Dyes. In *Solar Cells - Dye-Sensitized Devices*, 2011.
9. Green, A. N. M.; Palomares, E.; Haque, S. A.; Kroon, J. M.; Durrant, J. R., Charge Transport versus Recombination in Dye-Sensitized Solar Cells Employing Nanocrystalline TiO_2 and SnO_2 Films. *J. Phys. Chem. B* **2005,** *109* (25), 12525-12533.

10. Liu, L., Wang, H., Wang, D., Li, Y., He, X., Zhang, H., Shen, J., SnO@TiO_2 Core/Shell Nanowire Arrays with Different Thickness of TiO_2 Shell for Dye-Sensitized Solar Cells. *Crystals* **2020,** *10* (4), 325-334.
11. Grätzel, M., Dye-sensitized solar cells. *J. Photochem. Photobiol. C* **2003,** *4* (2), 145-153.
12. Negi, S. S., Integrated Electronic, Optical, and Structural Features in Pseudo-3D Mesoporous TiO_2-x Delivering Enhanced Dye-Sensitized Solar Cell Performance. *ACS Omega* **2018,** *3* (2), 1645-1652.
13. Boschloo, G., Improving the Performance of Dye-Sensitized Solar Cells. *Front. Chem.* **2019,** *7*, 77.
14. Baghel, S., Jha, R., Jindal, N., Material Selection for Dye Sensitized Solar Cells Using Multiple Attribute Decision Making Approach. *J. Renew. Energy* **2014,** *14*, 1-7.
15. Balgude, S.; Sethi, Y.; Kale, B.; Amalnerkar, D.; Adhyapak, P., Sn_3O_4 microballs as highly efficient photocatalyst for hydrogen generation and degradation of phenol under solar light irradiation. *Mater. Chem. Phys.* **2019,** *221*, 493-500.
16. He, Y.; Li, D.; Chen, J.; Shao, Y.; Xian, J.; Zheng, X.; Wang, P., Sn_3O_4: A novel heterovalent-tin photocatalyst with hierarchical 3D nanostructures under visible light. *RSC Adv.* **2014,** *4* (3), 1266-1269.
17. Tanabe, T.; Hashimoto, M.; Mibu, K.; Tanikawa, T.; Gunji, T.; Kaneko, S.; Abe, H.; Miyauchi, M.; Matsumoto, F., Synthesis of Single Phase Sn_3O_4: Native Visible-Light-Sensitive Photocatalyst with High Photocatalytic Performance for Hydrogen Evolution. *J. Nanosci. Nanotechnol.* **2017,** *17* (5), 3454-3459.
18. Lawson, F., Tin Oxide-Sn_3O_4. *Nature* **1967,** *215*, 955-956.

19. Song, H.; Son, S.-Y.; Kim, S. K.; Jung, G. Y., A facile synthesis of hierarchical Sn_3O_4 nanostructures in an acidic aqueous solution and their strong visible-light-driven photocatalytic activity. *Nano Res.* **2015,** *8* (11), 3553-3561.

20. Karlsson, M., Jogi, I., Eriksson, S. K., Rensmo, H., Boman, M., Boschloo, G., Hagfeldt, A., Dye-sensitized Solar Cells Employing SnO_2-TiO_2 Core-shell Structure Made by Atomic Layer Deposition. *Sol. Energy Harvesting* **2013,** *67* (3), 142-148.

21. Huang, J., Chiu, S., Wu, M., Hsu, C., Effect of titanium oxide compact layer in dye-sensitized solar cell prepared by liquid-phase deposition. *Appl. Phys. A.* **2016,** *122* (11).

22. Andrew Lyon, L.; Hupp, J. T., Energetics of the Nanocrystalline Titanium Dioxide/Aqueous Solution Interface: Approximate Conduction Band Edge Variations between H_o=-10 and H_-=+26. *J. Phys. Chem. B* **1999,** *103* (22), 4623-4628.

23. Chen, G., Ji, S., Sang, Y., Chang, S., Wang, Y., Hao, P., Claverie, J., Liu, H., Yu, G., Synthesis of scaly Sn_3O_4/TiO_2 nanobelt heterostructures for enhanced UV-visible light photocatalytic activity. *Nanoscale* **2015,** *7*, 3117-3125.

24. Yu, J.-G.; Yu, H.-G.; Cheng, B.; Zhao, X.-J.; Yu, J. C.; Ho, W.-K., The Effect of Calcination Temperature on the Surface Microstructure and Photocatalytic Activity of TiO_2 Thin Films Prepared by Liquid Phase Deposition. *J. Phys. Chem.* **2003,** *107* (50), 13871-13879.

25. Rho, W.-Y.; Jeon, H.; Kim, H.-S.; Chung, W.-J.; Suh, J. S.; Jun, B.-H., Recent Progress in Dye-Sensitized Solar Cells for Improving Efficiency: TiO_2 Nanotube Arrays in Active Layer. *J. Nanomater.* **2015,** *2015*, 1-17.

26. Ahmadi, S., Asim, N., Alghoul, M.A., Hammadi, F. Y., Saeedfar, K., Ludin, N. A., Zaidi, S. H., Sopian, K., The Role of Physical Techniques on the Preparation of Photoanodes for Dye Sensitized Solar Cells. *Int. J. Photoenergy* **2014,** *2014*.

27. Maki, H.; Okumura, Y.; Ikuta, H.; Mizuhata, M., Ionic Equilibria for Synthesis of TiO_2 Thin Films by the Liquid-Phase Deposition. *J. Phys. Chem.* **2014,** *118* (22), 11964-11974.

28. Peiró, A. M.; Peral, J.; Domingo, C.; Domènech, X.; Ayllón, J. A., Low-Temperature Deposition of TiO_2 Thin Films with Photocatalytic Activity from Colloidal Anatase Aqueous Solutions. *Chem. Mater.* **2001,** *13* (8), 2567-2573.

29. Pham, B., Willinger, D., McMillan, N. K., Roye, J., Burnett, W., D'Achille, A., Coffer, J. L., Sherman, B. D., Tin(IV) Oxide Nanoparticulate Films for Aqueous Dye-Sensitized Solar Cells. *Submitted* **2021**.